NASA TECHNICAL MEMORANDUM NASA-TM-76647 19820006405 NASA TM-76647

ATTITUDE MEASUREMENT PRINCIPLES AND SENSORS

P. Duchon and M.P. Vermande

Translation of "La mesure d'attitude, les principes - les sensors", In: Le mouvement du vehicle spatial en orbit. Cours de Technologie Spatial (Spacecraft Orbital Motion; Course in Space Technology), Toulouse, France, June 2-13, 1980. Proceedings. Toulouse, Centre National d'Etudes Spatiales, 1980, pp. 315-348.

NATIONAL AERONAUTICS AND SPACE ADMINISTRATION
WASHINGTON, D.C. 20546 NOVEMBER 1981

STANDARD TITLE PAGE

1. Report No. NASA TM-76647	2. Government Accession No.	3. Recipient's Catalog No.
4. Title and Subtitle ATTITUDE MEASUREMENT - PRINCIPLES AND SENSORS		5. Report Date November 1981 6. Performing Organization Code
7. Author(s) P. Duchon and M.P. Vermande Centre National d'Etudes Spatiales		8. Performing Organization Report No. 10. Work Unit No.
9. Performing Organization Name and Address Leo Kanner Associates Redwood City, California 94063		11. Contract or Grant No. NASW-3541 13. Type of Report and Period Covered Translation
12. Sponsoring Agency Name and Address National Aeronautics and Space Administration, Washington, D.C. 20546		14. Sponsoring Agency Code

15. Supplementary Notes

Translation of "La mesure d'attitude, les principes - les sensors", In: Le mouvement du vehicle spatial en orbit. Cours de Technologie Spatial (Spacecraft Orbital Motion; Course in Space Technology), Toulouse, France, June 2-13, 1980. Proceedings. Toulouse, Centre National d'Etudes Spatiales, 1980, pp. 315-348. (A81-33388)

16. Abstract

Tools used in the measurement of satellite attitude are described. Attention is given to the elements that characterize an attitude sensor, the references employed (stars, moon, sun, earth, magnetic fields, etc.), and the detectors (optical, magnetic, and inertial). Several examples of attitude sensors are described, including sun sensors, star sensors, earth sensors, triaxial magnetometers, and gyrometers. Finally, sensor combinations that make it possible to determine a complete attitude are considered; the SPOT attitude measurement system and a combined CCD star sensor-gyrometer system are discussed.

17. Key Words (Selected by Author(s))	18. Distribution Statement
	Unclassified-Unlimited

19. Security Classif. (of this report)	20. Security Classif. (of this page)	21. No. of Pages	22.
Unclassified	Unclassified		

N82-14278#

NASA-HQ

CONTENTS

ATTITUDE MEASUREMENT PRINCIPLES AND SENSORS

P. Duchon and M.P. Vermande
Centre National d'Etudes Spatiales, Toulouse

1. Introduction

/316*

The purpose of this course is to inform the reader of the means currently used for measuring satellite attitude. After a brief description of an attitude sensor's characteristic elements, we shall describe the detectors that are currently the most familiar, with special emphasis on their operational specifications (measurement range, precision, stability) and applications.

We shall then succinctly describe the sensors now most widely used, or on the point of widespread use, and we shall finish the course with a few examples of sensor combinations for determining total attitude.

2. The Characteristic Elements of an Attitude Sensor

When faced with the multitude of sensors that have been built or studied, one feels the need to isolate their common essential elements. We shall distinguish between:

2.1 The Reference Source, Which Could Be[1]:

-- a star,
-- the moon,
-- the sun,

[1] It should be noted that one class of detectors uses a reference source that is especially linked to the phenomenon of inertia. These are gyroscopic detectors and accelerometers.

* Numbers in the margin indicate pagination in the foreign text.

-- several of the earth's features:
  + the visible albedo,
  + the infrared horizon,
  + a beacon,
-- the magnetic field,
-- a radio source.

2.2 The Vehicle's Movement

-- Attitude: spinning,
  three-axis stabilized
-- Orbit: inclination, eccentricity, and semimajor axis.

2.3 Operational Specifications

-- measurement range,
-- precision,
-- lifespan,
-- characteristics of output signal,
-- interface with vehicle:
  + bulkiness, weight,
  + fuel consumption
  + signal processing (on-board computer)

2.4. The Techniques Used in the Subsystems

-- optics
-- detection,
-- modulation,
-- signal processing.

We shall go into more detail below on two points: reference sources and detectors.

3. Reference Sources

/317

3.1 Stars

Advantages to Using Them as Reference Directions:

-- They are numerous;
-- they look like bright points, so that the reference direction is perfectly defined;
-- their direction is practically "inertial", which is not the case for the sun's direction (over periods on the order of or more than a day).

Disadvantages

-- The available energy is low -- the brightest stars produce an illuminance of less than 10^{-12} W/cm^2;
-- there is consequently a high risk of interference from spurious fluxes (the sun's light, albedo, the moon, etc.).

Magnitude of a Star

Let E be the spectral illuminance produced by a star at 5500 Å. The difference in visual magnitude between two stars is defined as:

$$m_{v_1} - m_{v_2} = 2.5 \log_{10}(E_2/E_1).$$

E can be expressed in, for example, erg/cm^2/sec/Å, i.e., in ergs (radiant energy) per cm^2 of receiving surface normal to the beam per second per Angstrom of band width.

Now that the scale is determined, it is necessary to define a zero point.

By convention, the visual magnitude is zero if the spectral illumination is 4×10^{-9} erg/cm^2/sec/Å. At 5500 Å, this is equivalent to 1,000 photons/cm^2/sec/Å.

Statistical Distribution of Magnitudes

A statistical table can be drawn up to give an idea of the abundance of stars in the sky. This table shows the probability of finding a star in the heavens that has a magnitude lower than a certain value m and is within a given one square degree solid angle.

Magnitude m	Probability of finding a star with a magnitude less than "m" inside 1 sq. degree
7	0,31
6	0,12
5	0,04
4	0,013
3	0,0014

The heavens as a whole cover approximately 41,000 square degrees. Naturally, the abundance of bright stars depends on the celestial zone under consideration.

The brightest stars: /318

Sirius	$m_v = -1.43$
Canopus	$m_v = -0.71$
Achernar	$m_v = -0.28$
α Centauri	$m_v = -0.27$
...	
Polaris	$m_v = 2.1$

The stars are also grouped into spectral classifications according to their apparent temperatures.

Each classification is divided into ten subgroups. The lowest number subgroup has the highest temperature. Example:

Class F_0 = 7500°K.

Type	W O	B	A	F	G	K	M
Temperature °K	70 000	38 000	15 000	8 000	6 000	5 000	3 500

Choice of Reference Star

The choice of star depends on the case at hand, and various constraints must be taken into consideration. These include: geometrical constraints (for example, choice of a reference direction approximately perpendicular to the axis of rotation) and detection constraints (magnitude as low as possible and convenient location in the heavens, with no nearby star that might cause confusion).

Finally, the existence of a multitude of dim stars not resolved by any instrument and constituting a kind of continuous background noise must not be forgotten.

The average luminance of this continuous background noise is 10^{-15} watt/cm^2 - deg^2 (or 4.125 x 10^{-7} W x m^{-2} x sr^{-1}).

3.2 The Moon

Characteristics

-- Apparent diameter: from 27'30" to 32'45".

-- Low reflectivity: from 0.07 to 0.16 according to the wavelength. The moon's brightness comes from reflected solar light.

-- Full moon: an illuminance which is a few millionths that of the sun outside the atmosphere: 3 x 10^{-7} W/cm^2 - deg^2 (or 1.24 x 10^2 W x m^{-2} x sr^{-1}).

The major characteristic of lunar radiance is its variation with phase. The illuminance curve has a very sharp maximum when the

moon is full and decreases very rapidly afterwards (faster than if the moon were a perfect diffuser).

/319

Phase	before full moon	after full moon
0°	1	1
10°	0,78	0,76
20°	0,60	0.58
30°	0.46	0,45
40°	0.36	0.35
50°	0,27	0,27
60°	0,21	0,21
70°	0,16	0,16
80°	0,12	0,11
90°	0,08	0,08
100°	0,056	0,058

Difficulties with Using the Moon as a Reference Source

-- Large, rapid variations in its luminous intensity.

-- Relatively short distance away (causing a parallax effect in low orbit).

These two disadvantages are important for a satellite mission. They are negligible for a space probe.

Finally, the moon's emission is not uniformly distributed over the disk (crescent, etc.) and therefore the direction detected by the sensor (generally the barycenter of luminous intensities) is not the direction of the moon's center.

3.3 The Sun

General Comments

The sun is the most intense source in the sky and the simplest to use. Solar energy is abundant, especially in the visible wavelengths, for which excellent detectors are available. In addition, the sun's angular breadth is fairly small (0.5°), so the reference direction is relatively well defined.

Characteristics

-- Average earth-sun distance: 150,000,000 km.

-- Apparent diameter when seen from the earth: from 31'28" to 32'32" as a result of the ellipticity of the earth's orbit.

-- Flattening: 0.0017.

The minimum distance between the earth and the sun (perihelion) occurs in the beginning of January.

For the same reasons, the solar illuminance reaching the earth's atmosphere varies during the year by about $\pm$ 3.4%. /320

The sun's emission is close to that of a black body at 6,000°. It therefore reaches a maximum at around 0.55 microns, and a fairly broad portion of the spectrum is in the visible and near infrared sectors.

Roughly, the sun seems to be a uniformly bright disk even though a more detailed analysis shows that at certain wavelengths, the center is brighter than the edges, and that the opposite is true for others.

The sun's luminance is $2 \times 10^{+7}$ $W\text{-}m^{2}\text{-}sr^{-1}$.

The luminance is much less at ground level because of atmospheric absorption. Precise calibrations on the ground are therefore relatively difficult.

3.4 The Earth

2.4.1 The Albedo

The albedo is the light the earth sends back into space. There is a coefficient of albedo defined as:

$$\frac{\text{Quantity of reflected and diffused solar energy}}{\text{Quantity of incident energy}}$$

On the average, it is equal to: 39% for visible light,
28% for near infrared,
50% for UV.

The earth's luminance in these wavelengths is not uniform:
-- effect of night and day,
-- changes in the cloud cover.

The earth is therefore not used very much as a reference source.

However, it has been proposed that the luminance's inhomogeneity can be used as the basis of a "fishbone"-type yaw sensor.

The average luminance of the earth's lighted zones is on the order of 150 W m^{-2} sr^{-1}.

3.4.2 The IR Horizon

3.4.2.1 Albedo and Emission

We have seen that part of the radiation coming from the sun is sent back into space. However, diffusion is attenuated very rapidly in the infrared region of the spectrum, and the albedo is negligible for wavelengths greater than 2 or 3 microns.

In contrast, the atmosphere and the earth radiate according to Kirchhoff's law:

$$E_\lambda = a_\lambda B_{(\lambda,T)},$$

where a_λ = the coefficient of absorption of the body under consideration at wavelength λ; $B_{(\lambda,T)}$ = a black body's spectral luminance at wavelength λ and at temperature T of the body under consideration.

The temperature of the earth and of a large proportion of the atmosphere is in the vicinity of 300°K, and therefore maximum emission is located at around 10 microns. However, in reality, earth + atmosphere do not behave like a gray body and the observed emission varies greatly as a function of wavelength.

3.4.2.2 The Earth-Space Contrast in the 14-16.3 Micron IR Spectral Band /321

This is the CO_2 absorption band.

We shall deliberately limit ourselves to the 14-16 micron spectral band as the majority of earth-oriented detectors use it. The terrestrial atmosphere's emission varies little in this spectral region for changing seasons and locations. In other words, a detector working in the 14 to 16 micron band "sees" the earth in the same way whatever the period of the year. In addition, as far as the 14-16 micron band is concerned, the geometry of the earth can be reduced to that of a surface coinciding with the level of the oceans (geoid).

It is in fact advantageous to base measurements of attitude relative to the earth on the terrestrial horizon. In the case of high altitude orbits (10,000 km or more) approximating the geoid by a sphere is sufficient. For low orbits or if a precision on the order of 0.1° in geocentric coordinates is desired, it is necessary to take account of the oblateness of the earth. The earth can then be approximated by an ellipsoid with a north-south axis of revolution, a flattening of 1/297, and a semi-major axis of 6,378 km (radius at the equator).

Note: The so-called "pear" effect can be neglected since it corresponds to variations from the ellipsoid of only ± 14 m. In figures 1a and 1b, we have plotted the horizon profiles in the 14-16.3 micron region (luminance as a function of altitude for a space-borne observer looking at the earth's horizon) at a latitude of 20° N (figure 1a) and 75° N (figure 1b) and at different times of the year (July, October, January, and April).

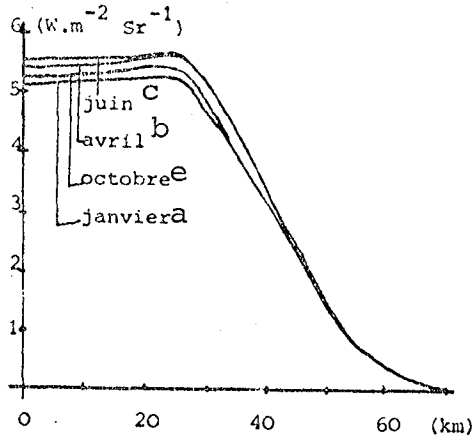

Figure 1a
20° North Latitude

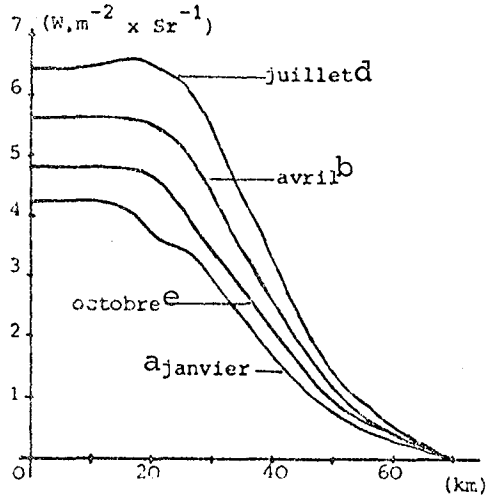

Figure 1b
75° North Latitude

Horizon Profiles
615-715 cm^{-1} Band

Key: a) January
b) April
c) June
d) July
e) October

Bear in mind that the maximum and minimum luminance in summer or winter is at the North and South Poles. The ratio between maximum and minimum luminance is greater than 2. Also, the variations in the luminance profiles are mainly a function of the season and the latitude. Nevertheless, random variations of ± 10% can be observed at different longitudes (along a given parallel). /322

3.5 The Magnetic Field

We shall not go into the different possible models for the earth's magnetic field very deeply.

Nevertheless, it is necessary to mention that while this reference source is stable at low altitudes (less than 1000 km), with precision on the order of or less than 1°, this is not true for geostationary orbits. Thus, magnetometers can help determine (to the nearest degree) part of the attitude of a body to which they are attached if the body is in low-earth orbit. However, in geostationary orbits, the deformation of the magnetic field by the solar wind makes their use impossible.

3.6 Radio Sources

(For memory)

4. Detectors

4.1 Optical Detectors

The basic component of an optical sensor is the detector. The design of the sensor is based on it and its specifications.

4.1.1 Visible Light Detectors

4.1.1.1 Silicon Photodiodes

Silicon photodiodes are very widely used. They are sensitive to light ranging from the UV to the near IR.

An n- (or p-) doped layer is formed on a p- (or n-) doped silicon substrate so as to create an np junction.

The I-V characteristic of this diode shifts along the I-axis in proportion to the flux ϕ arriving at the junction.

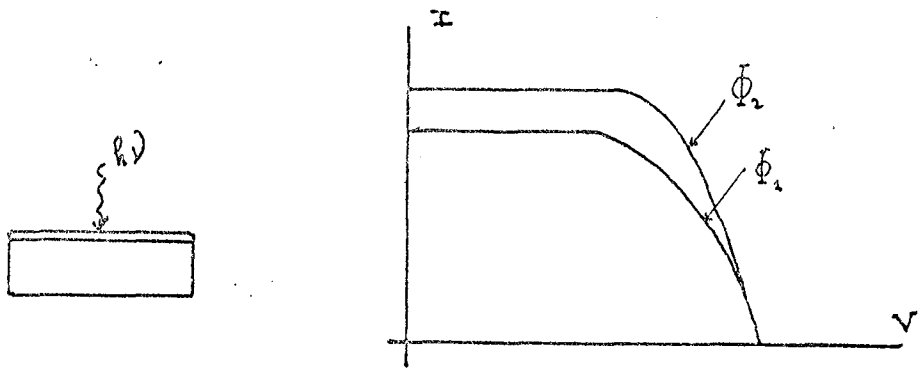

Figure 2

For a charge resistance less than a certain limit, the current I /323 is proportional to ϕ. The dimensions of photodiodes vary greatly. Their configurations can be very different, also: simple element, matrices, very elongated rectangular elements (digital solar sensors), etc.

The silicon photodiode is the detector used in sun sensors. The signal is very convenient. A 1 cm^2 cell exposed perpendicularly to the sun's rays outside the atmosphere has a characteristic curve passing through the points:

V = 0, I = 30 mA

I = 0, V = 500 mV.

Very low noise photocells exist. They can be used to detect a star.

Example: Signal-to-noise ratio in the case of a star of magnitude 5, a 100 cm^2 lens and a diode whose PEL = 6×10^{-1}.

The illuminance E_1 of a star of magnitude $m_{V_1} = 5$ confirms:

$$m_{v_2} - m_{v_1} = 2.5 \log_{10} (E_2/E_1),$$

in which for $m_{v_2} = 0$, $E_2 = 4 \times 10^{-12}$ W x m^{-2} x $\mathring{A}^{-1}$ at 5500 Å.

$E_1 = 4 \times 10^{-14}$ W x m^{-2} x $\mathring{A}^{-1}$.

The energy arriving at the detector is, for $\Delta\lambda$ = 5000 Å:
$4 \times 10^{-14} \times 5000 \times 10^{-2} = 20 \times 10^{-13}$ W.

The signal-to-noise ratio = $\frac{20 \times 10^{-13}}{6 \times 10^{-13}} \approx 3$ for Δf = 1 Hz.

4.1.1.2 Photomultipliers

4.1.1.2.1 Description and Operating Principles

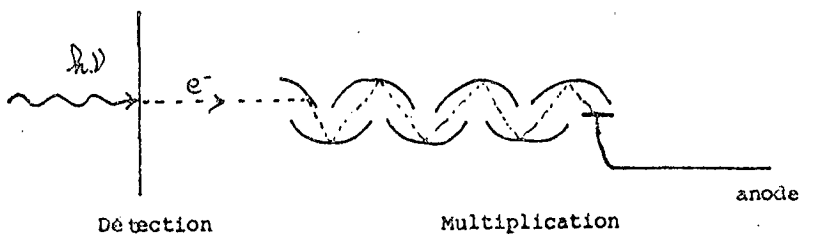

Figure 3
Multiplication of Electrons by
Secondary Emission at Each Dynode

4.1.1.2.2 Sensitivity Depends on the Type of Photocathode /324

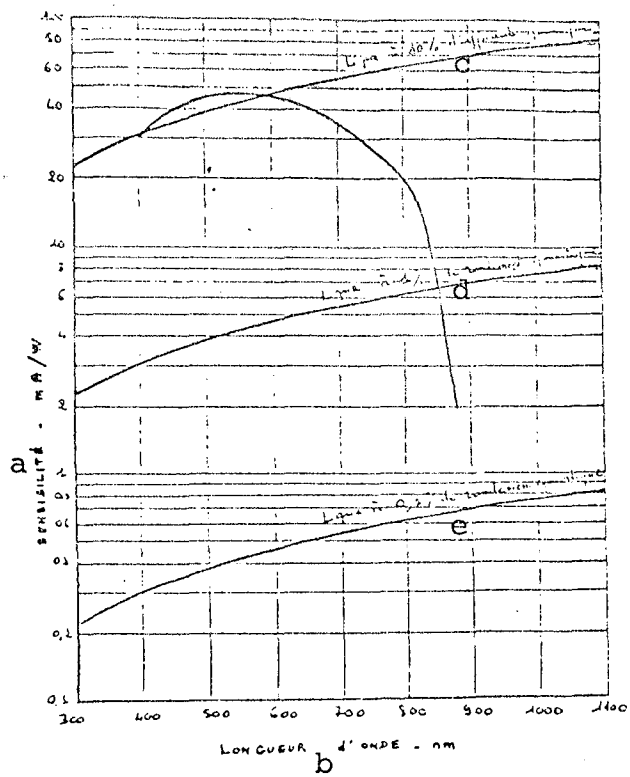

Figure 4
Typical Spectral Response of an S20R Photocathode

Key: a) Sensitivity -- mA/W
b) Wavelength -- nm
c) Line at 10% quantum efficiency
d) Line at 1% quantum efficiency
e) Line at 0.1% quantum efficiency

4.1.1.2.3 Output Signal /325

Let F be the input flux in watts, η the photocathode's sensitivity in A/W, and K the electron collection efficiency in the multiplying section.

The gain in the multiplying section is $G = \delta^n$, where δ is the gain in one multiplier stage, typically $\delta = 3$ to 5 and n is the number of stages in the multiplier, $6 \leq n \leq 14$.

The useful output signal is:

$$I_{s_{output}} = F\eta K\delta^n$$

The signal hitting the first dynode is then:

$I_s = F\eta K$

4.1.1.2.4 Noise Level

Two principal sources:

-- Fluctuations in the signal and dark current. They are at their maximum level prior to the first multiplying dynode.

-- Fluctuations in the secondary emission gain at the dynodes. The influence of the first dynode is preponderant.

The input equivalent of the downstream electronic noise is negligible provided that the gain is high.

$$\langle i^2_{noise} \rangle = 2q(I_o + I_s) \cdot \Delta f \cdot \frac{\delta}{\delta - 1}$$

where Δf = noise band (Hz), I_s is the signal current at the first dynode, and I_o is the dark current striking the first dynode.

$\delta/\delta-1$ = the noise factor of the multiplying section.

$I_o < 2 \times 10^{-16}$ A/cm^2 for a photomultiplier with an S 20 photocathode at 20°C.

4.1.1.2.5 Signal-to-Noise Ratio

If I_o is negligible in comparison with I_s:

$$\frac{S}{N} = \frac{I_s}{\sqrt{2q\,(I_o + I_s).\Delta f . \frac{\delta}{\delta - 1}}}$$

$$\frac{S}{N} = \sqrt{\frac{F\eta}{q} \cdot \frac{1}{2 \cdot \Delta f} \cdot \frac{\delta - 1}{\delta}}$$

$$\frac{S}{N} = \sqrt{F'\eta \cdot \frac{1}{2\Delta f} \cdot \frac{\delta - 1}{\delta}} \qquad \left(F' = F/q \right)$$

4.1.1.3 Image Dissector

4.1.1.3.1 Description and Operating Principles

This is a deflectable photomultiplier.

The photocathode output is the electronic image of the scene. The image passes before one or several apertures behind each of which is a multiplying section analogous to that of a photomultiplier.

The quality of the electronic focusing optics and the size of the aperture define the tube's resolution.

See the schematic drawing of an image dissector tube in figure 5.

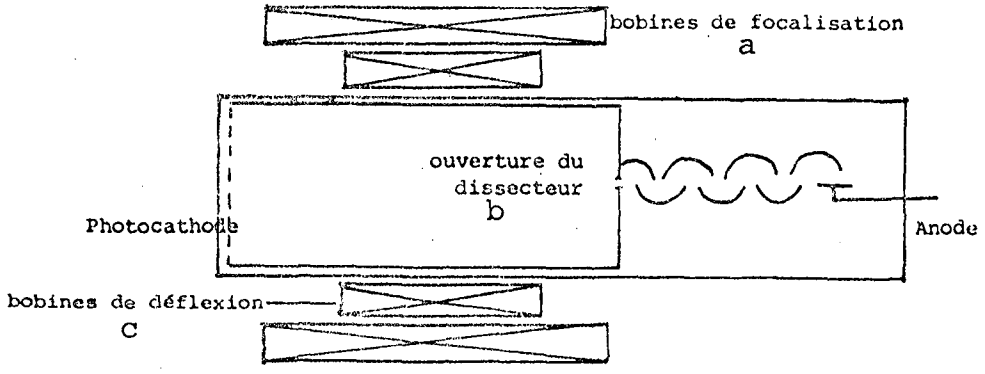

Figure 5

Key: a) Focusing Coils
b) Dissector Aperture
c) Deflecting Coils

4.1.1.3.2 Output Signal

4.1.1.3.3 Sensitivity

4.1.1.3.4 Noise Level

For a dissector with n holes, the noise is divided by $\sqrt{n}$.

4.1.1.3.5 Signal-to-Noise Ratio

For a dissector with n holes the S/N ratio is multiplied by $\sqrt{n}$.

4.1.1.3.6 Modulation Transfer Function (MTF)

The limits of resolution in a dissector with electromagnetic reflection focusing are excellent, up to 65 to 75 lp/mm. /327

4.1.1.4 Charge Transfer Semiconductor Arrays and Rows

Such arrays function by accumulation and transfer of charge. They are usually photodiode networks, especially CCD (charge coupled device) and CID (charge injection device) rows and mosaics. Such elements have an advantage over image dissector tubes in that they are practically insensitive to outside elements. Image detectors, on the other hand, require cooling if stars with a magnitude of more than four are to be detected.

Image dissectors also have the disadvantage of degrading in the presence of high energy particles.

A CCD array works similarly to a row of elements. Charge transfer is accomplished on a transfer mosaic (memorization). The image is then read line by line (with the transfer mosaic playing the role of a two-dimensional shift register. /328

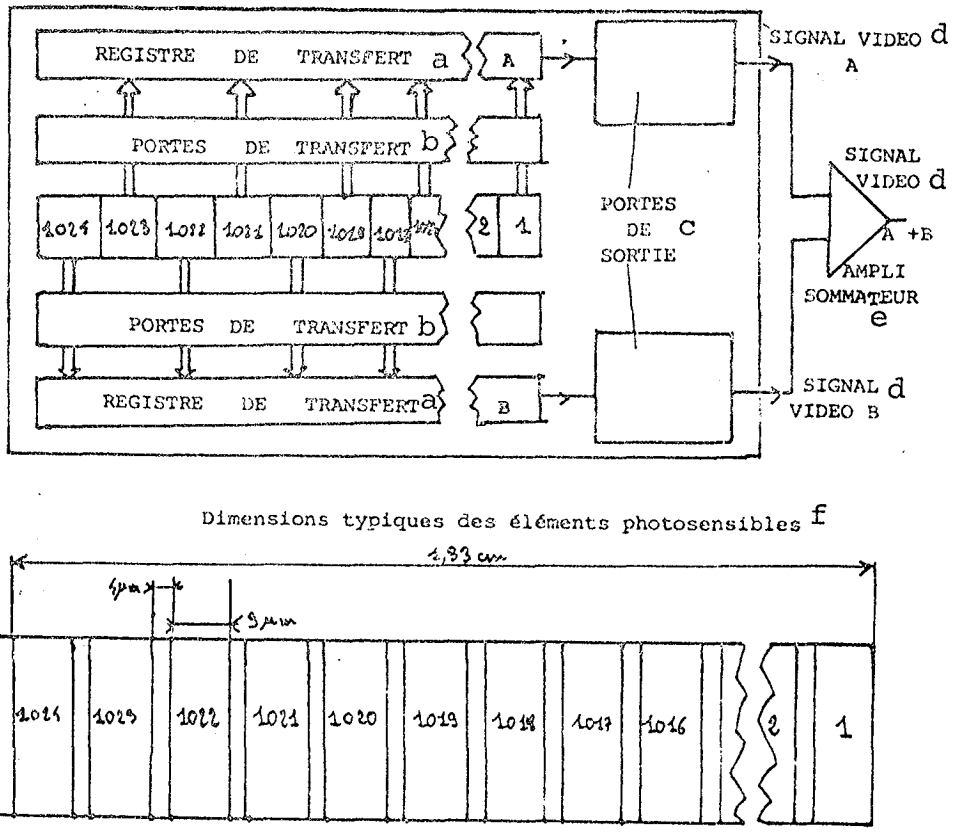

Figure 6
Schematic Drawing of a 1024 Element CCD-Type Detector

Key:
a) Transfer Register
b) Transfer Gates
c) Output Gates
d) Video Signal
e) Summing Amp
f) Typical Dimensions of Photosensitive Elements

4.1.2 Infrared Detectors

A large number of quantum detectors are not usable in attitude sensors because they have to be cooled to a temperature equal to or less than 77°K.

All that is left are thermal detectors, i.e. those whose signal is related to variations in the temperature of the sensitive element. There are:

-- Thermovoltaic detectors: They behave like voltage generators and are either thermocouples or thermopiles.

-- Nonthermovoltaic detectors:

+ bolometers, whose resistance varies with temperature;
+ pyroelectric detectors, whose capacitance varies with temperature.

Pneumatic detectors are not used as their operating principles are poorly adapted to outer space.

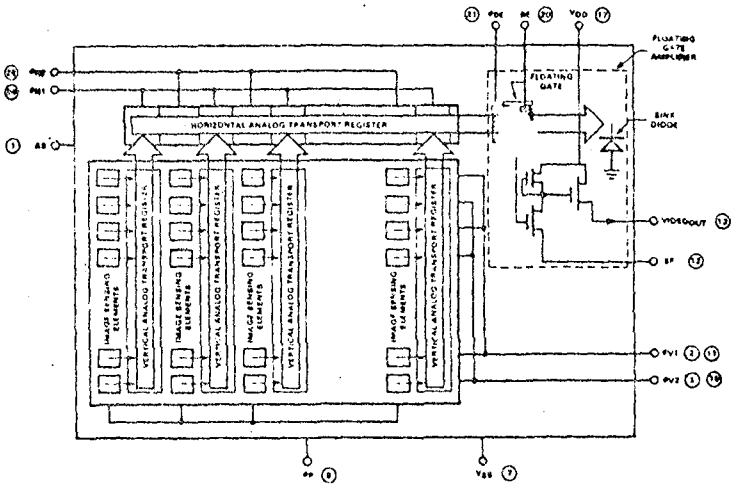

Figure 7
CCD Array -- Principle of Operation

4.1.2.1 Bolometers

The resistance of the sensitive element varies with temperature. So as to be independent of the ambient temperature, a differential measurement is made. The radiation to be measured hits only one of two side-by-side elements. The polarization voltage is on the order of 50 V.

The pulse response decreases very slowly, and the signal does not reach zero until after ten milliseconds have elapsed. Thus, sensitivity decreases very rapidly with increasing frequency (figure 8).

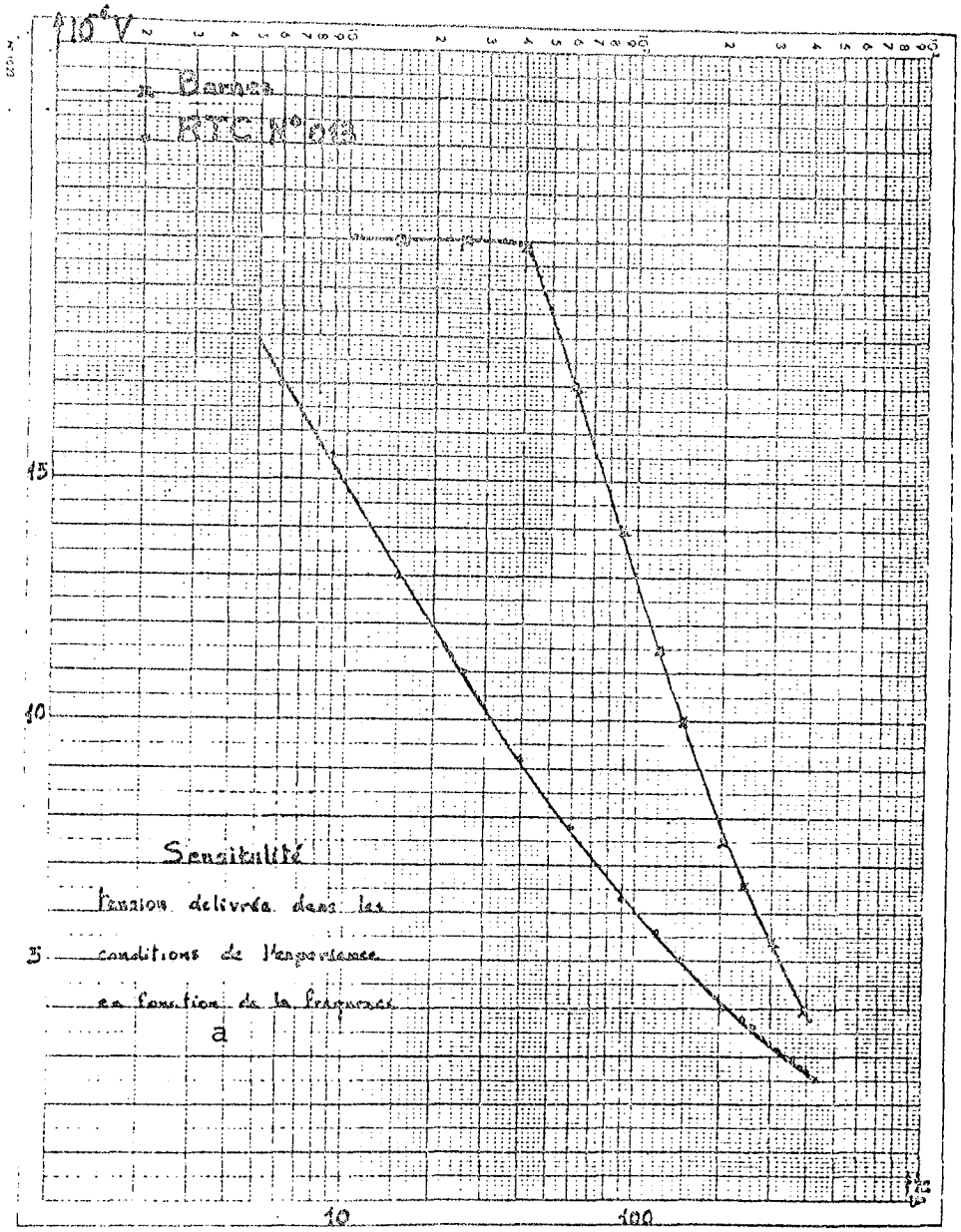

Figure 8

Key: a) Sensitivity: Voltage produced in experimental conditions as a function of frequency

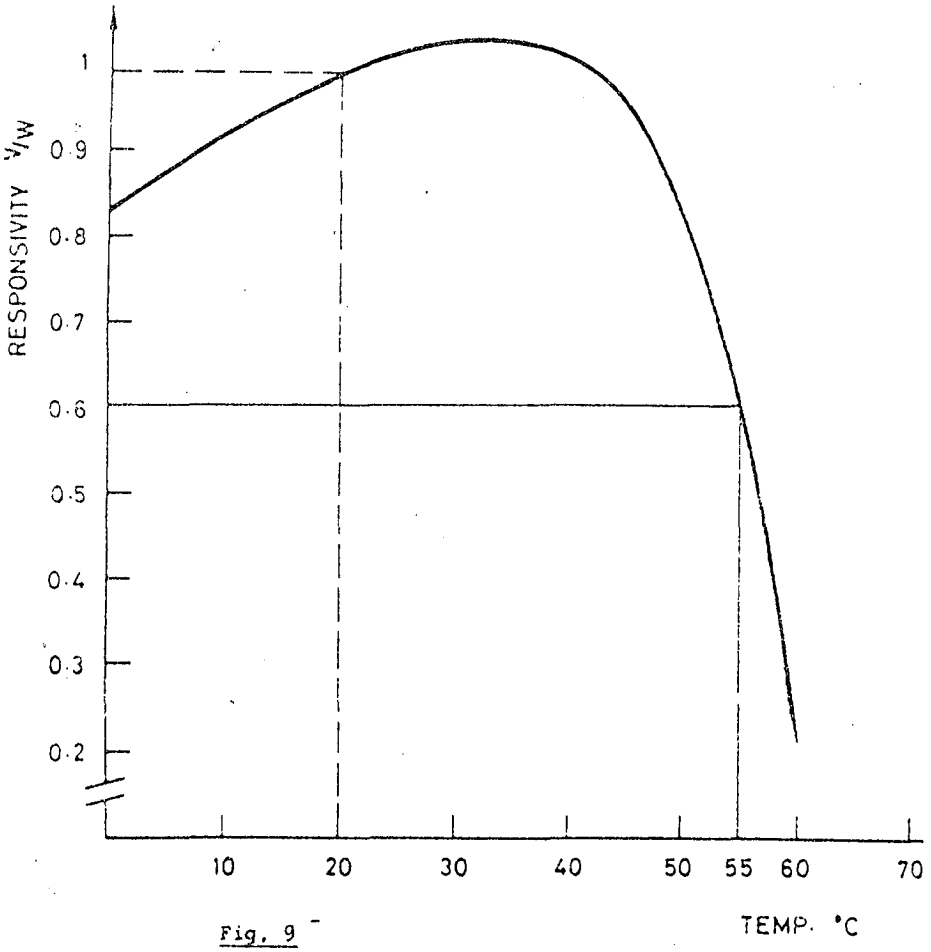

Fig. 9 - RESPONSIVITY VS TEMPERATURE

A4/4/5973

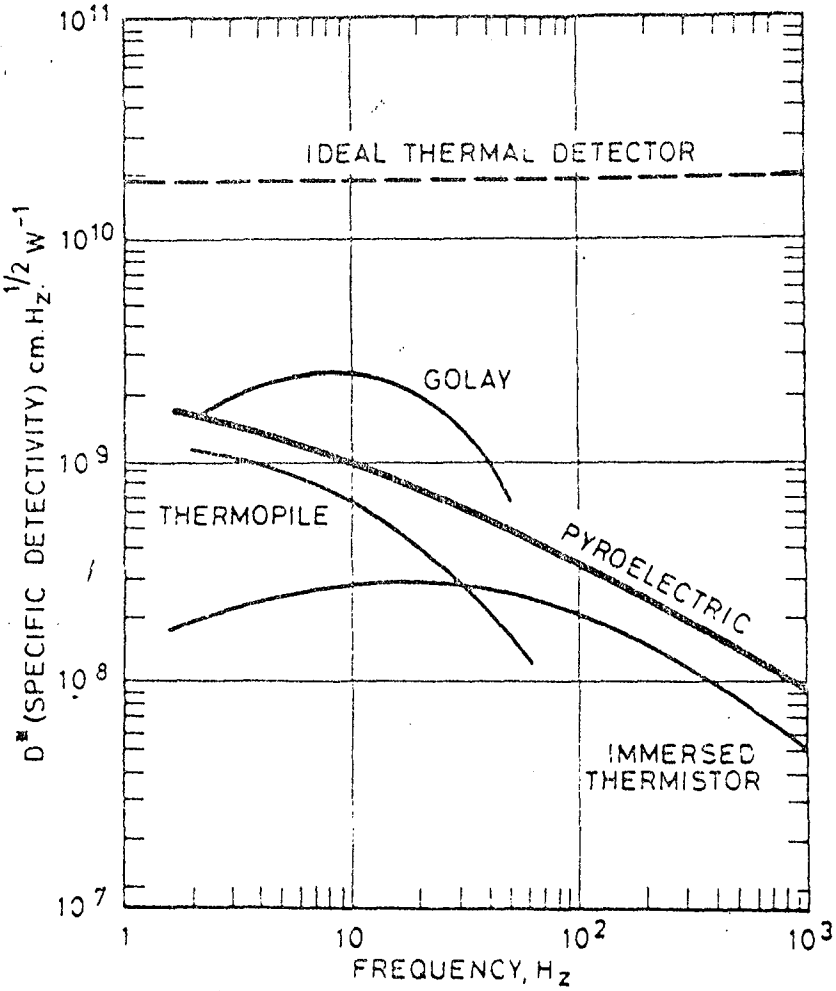

FIG.10. D^* (SPECIFIC DETECTIVITY) VERSUS FREQUENCY FOR THERMAL INFRARED DETECTORS

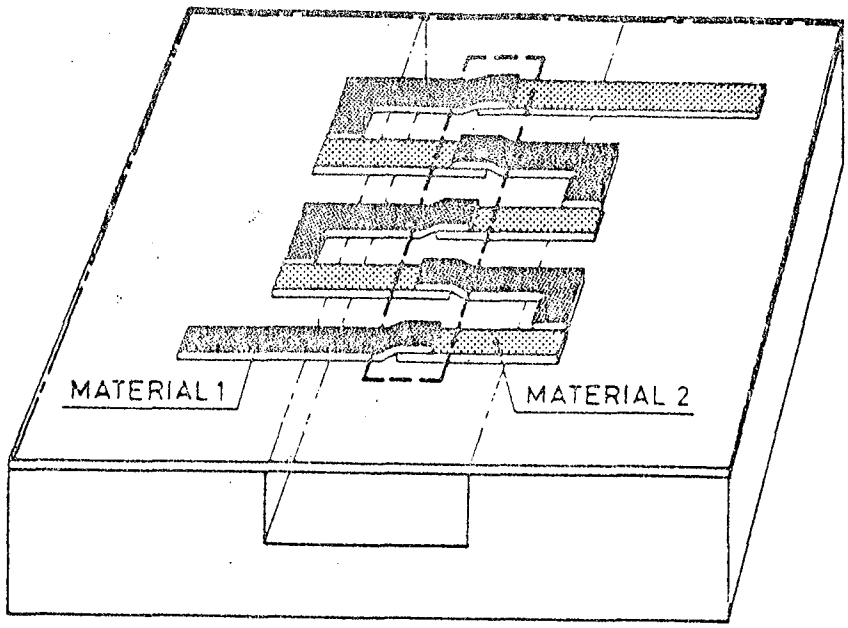

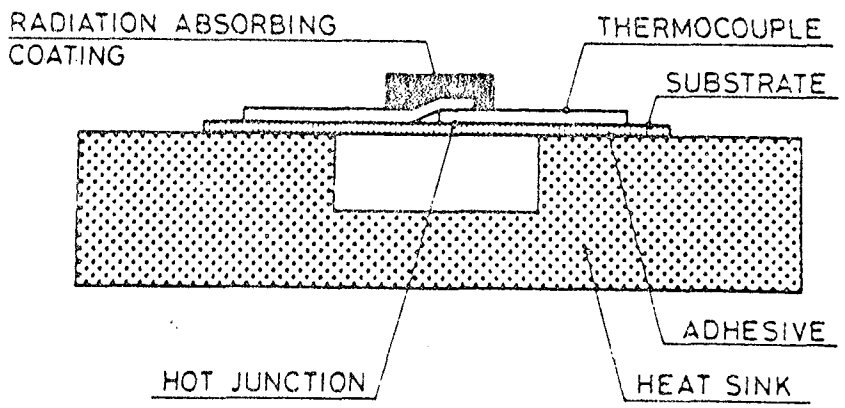

FIG.11-THIN FILM THERMOPILE

Noise, on the other hand, rapidly increases as low frequencies (less than 100 Hz) are approached. /333

The overall PEL has a minimum at around 100 Hz. It is then on the order of a few 10^{-9} $W/\sqrt{Hz}$.

Detectivity can be improved by immersing the bolometer. This procedure consists in placing the sensitive element in a medium with a high index (4 for germanium). Since the size of the beam remains constant, the same amount of energy is absorbed with a detector n^2 times smaller. As noise varies with the square root of surface area, the signal-to-noise ratio is improved by a factor of n.

4.1.2.2 Pyroelectric Detectors

The operating principle here is to use the variations in the dielectric constant as a function of temperature. Measurements of the variations in capacitance are therefore made. The most used substance for these detectors is TGS (triglycene sulfate).

The major disadvantage of pyroelectric detectors is that they become inoperable if their temperature exceeds the Curie point, or about 50°C.

Figures 9 and 10 show sensitivity as a function of temperature and detectivity as a function of frequency.

4.1.2.3 Thermopiles (Figure 11)

Two thermoelectric materials alternate to form a serpentine coil. Every other junction is located either:

-- above the groove; in this case they are well insulated thermally from the heat sink; or
-- outside of the groove; in this case, they remain at the heat sink's temperature.

The incident radiation heats the junctions located above the groove (they are called hot junctions) and a voltage appears at the ends of the coil.

Detectors with a large surface area can be made by making a heat sink with several side-by-side grooves.

The major characteristic of this type of IR detector is that it can function without modulation, whereas for the others a signal modulation frequency of a few tens of hertz is needed.

When the thermoelectric substances are n- and p-doped bismuth telluride (Bi_2Te_3), the Seebeck coefficient is on the order of 200 $\mu V/°C$ and the noise is 1.5 to 2 times greater than the Johnson noise. Thermopiles on the order of a cm^2 can be built in this way with a sensitivity on the order of 30 V/W and an impedence of a few tens of kilohms.

A variant of this type of detector is the digital thermopile. Parallel slits are put in the substrate on which the thermoelectric substances are deposited. The part between two successive slits constitutes a thermopile which is independent of its neighbors.

When aluminum is used as the substrate, 15 micron slits spaced 100 microns apart can be made. Five digit thermopiles 300 microns wide have been developed.

4.2 Magnetic Detectors (for Example, Fluxgate-Type Crouzet Detector) /334

Basic Principle

A coil carrying a high-frequency excitation current exhibits dissymmetries in the terminal voltages induced by the variations of the alternating field when the sensor (with a ferromagnetic core) is subjected to an external field. A direct current is then reinjected into the coil to reestablish symmetry.

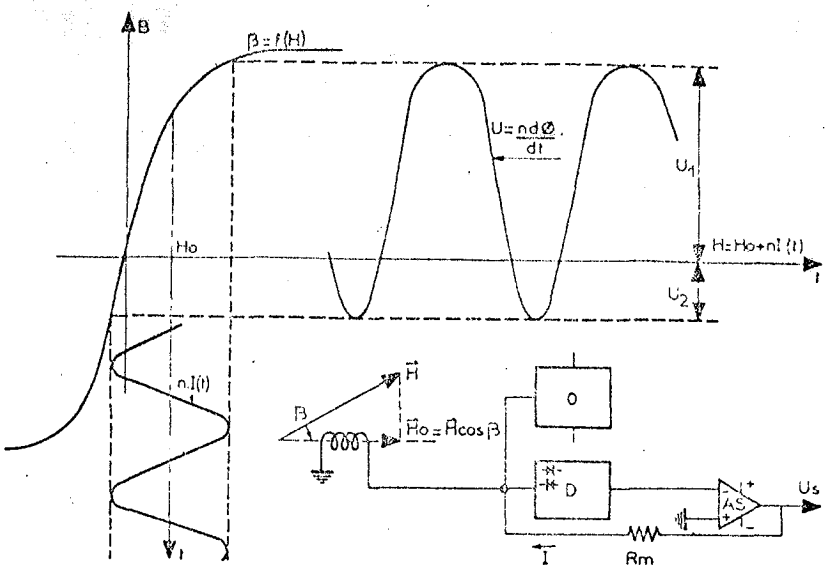

The current is proportional to the field being measured and, after the appropriate transformation, constitutes the output measurement.

4.3 Inertial Detector

4.3.1 The Floating Gyroscope: Operating Principles

A rotor (mounted on pivots) with an angular momentun H (maintained by a motor) is contained within a sealed housing. The unit, called a floating body, is immersed in a high density liquid which keeps it afloat and dampens its motion (see figure 12).

The detector contains three axes: the spin axis (s), the input or measurement axis (i), and the output axis (o).

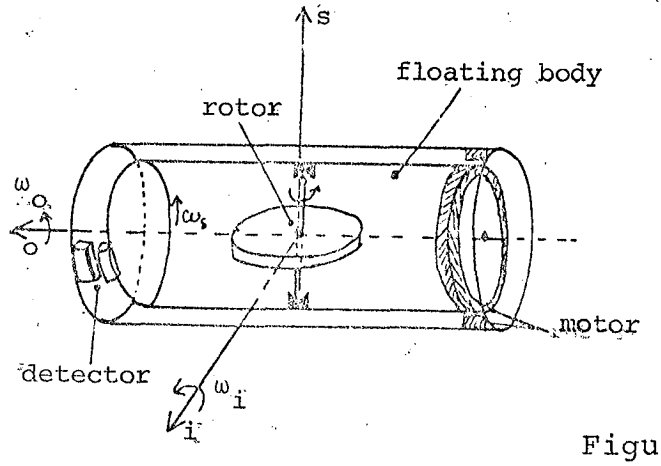

(The torque motor can be replaced by a passive torsion device in sensor gyros, which are in general more sturdy.)

Figure 12

According to the fundamental theorem of dynamics, an angular movement with a speed ω_i around the input axis produces a torque on the output axis, $\Gamma = H\omega_i$. /335

The dampening torque $f\omega_o$ and the inertial torque $Id\omega_o/dt$ oppose the gyroscopic torque in such a way that at equilibrium and in the presence of a motive torque Γ_m, the gyroscope equation (open loop) is:

$$H\omega_i - I\ (d\omega_o/dt) - f\omega_o - \Gamma_m = 0$$

If the motive torque Γ_m is zero, $\omega_i = f\omega_o/H$ in steady state, neglecting the effects of the time constant I/f. This is useful for the measurement of weak angular deflections, since $\Delta\theta_i = f\Delta\theta_o/H$.

In the majority of cases, the detector is recoupled to the motor by an electronic servocontrol circuit. This is the case for rate gyros, which measure angular velocity, or for digital gyroscopes reset by torque impulses such that $\Delta\theta_i = \Gamma_m\Delta t/H$.

Finally, the servocontrol loop is replaced in certain cases by a passive system. This is the case for torsion bar (or wire) gyro sensors, in which the torque motor is replaced by a restoring torsion proportional to the rotation of the floating body.

4.3.2 Dry (or Dynamically Tuned) Gyroscope

This is a nonfloating gyroscope with two degrees of freedom, whose inertial wheel is suspended by a turning, flexible joint. The joint allows the inertial wheel to pivot about two orthogonal axes (see figure 13). Two angular detectors (inductive, for example) produce a signal whose amplitude is proportional to the wheel's movement about the two perpendicular axes. The wheel-flexible joint assembly is tuned in such a way that when the wheel turns at a certain speed, the stiffness of the flexible joint balances the gimbal's inertial torque.

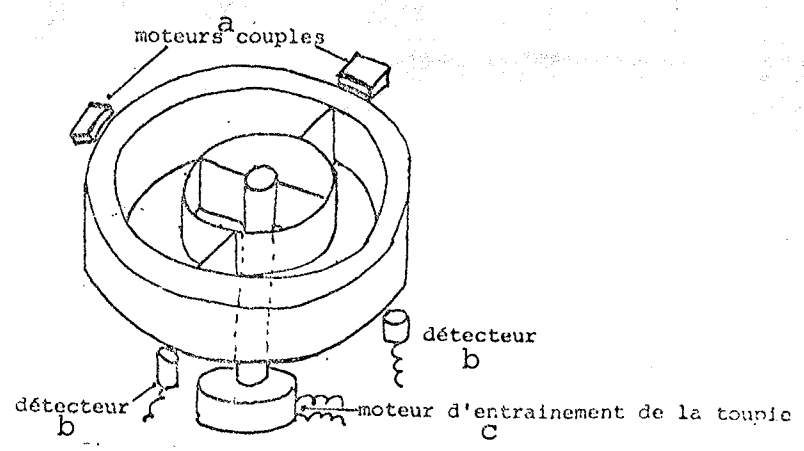

Figure 13
Basic Design of a Dynamically Tuned Gyroscope

Key: a) torque motors
b) detector
c) rotor motor

It is therefore possible to use this two-axis gyroscope in an angular deflection detector. In contrast, if the detectors are coupled to two torque motors placed on each axis of measurement, it is possible to use the detectors to measure angular velocity around each axis. A two-axis attitude sensor is thus obtained. /336

4.3.3 Accelerometer

We mention the accelerometer here just so that it will be kept in mind. It is in fact not much used for measuring actual attitude. However, it can be used for detecting the nutation of spinning satellites.

5. A Few Examples of Attitude Sensors

5.1 Sun Sensors

5.1.1 Examples of Analog Sun Sensors

A simple silicon cell can roughly provide the angle between its normal and the direction of sunlight. The precision obtained is on the order of 5 to 10°.

Slit Sun Sensors

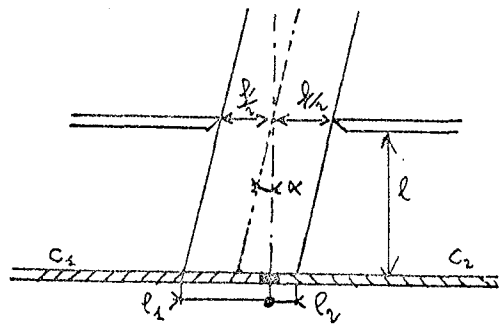

Figure 14

A diaphragm D contains a rectilinear slit behind which are placed two silicon photoelectric cells (figure 14).

The responses R_1 and R_2 of the cells C_1 and C_2 are of the form: /337

$$R_1 = K_1 \left(\frac{l}{2} + l.\mathrm{tg}\alpha\right) \cos\alpha$$

$$R_2 = K_2 \left(\frac{l}{2} - l.\mathrm{tg}\alpha\right) \cos\alpha$$

If the cells are homogeneous and identical, $K_1 = K_2 = K$, and the combination $R = \frac{R_1 - R_2}{R_1 + R_2} = \frac{2.l.\sin\alpha}{f.\cos\alpha} = \frac{2l}{f}\,\mathrm{tg}\alpha$ allows measurements of high accuracy, better than 0.5° in a ± 10° field.

Window Sun Sensors

The same technique as above is used, but to find the total direction of the sun, there are four cells and one window.

5.1.2 Digital Solar Sensors

Analog solar sensors work very well when used to make measurements around a zero point. It is helpful to describe a sensor's performance by its measurement quality: field of view ÷ precision within that field of view.

It is apparent that the measurement quality of analog solar sensors has a hard time exceeding 100. To obtain a figure of 1,000, digital sensors are necessary. The only limitations on their accuracy arise from defects in their geometry or optics or from source and quantization error.

Gray Code Digital Sensor

Solar sensors of this type make an overall measurement of the sun's direction. The sun's image through a slit (bar of light) is formed on sensitive silicon elements set up to have a Gray code (reflected binary code) output. A complementary sensitive track, covering the whole field of view, can be used to define the transition level (see figure 15).

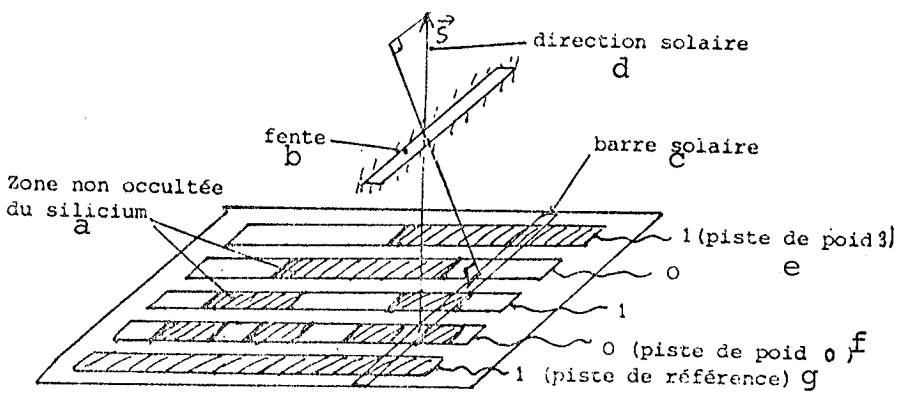

Figure 15
Schematic Drawing of a Digital Solar Sensor

Key: a) Nonocculted silicon zone
b) slit
c) bar of light
d) the sun's direction
e) track of weight 3
f) track of weight 0
g) reference track

Such a sensor therefore measures the dihedral angle between the plane formed by the sun's direction and the slit and the plane formed by the slit and a line passing through the slit and normal to the cells. /338

This type of sensor has been built in both Europe and the USA:

-- Leitz sensor for Symphonie (± 64° field around the measurement axis and ± 60° along the other axis, 0.5° resolution);
-- Sodern-SSDO2 Sensor for SRET II;
-- Adcole sensor (USA) with complementary offset tracks making it possible to attain a precision of one arc minute in a 64° field of view.

Digital Solar Sensor Containing a Row of Independent Detecting Elements (CCD, for Example)

Such a sensor was used in the ANS satellite (Dutch). The light-detecting row contained 200 elements. A similar sensor is planned for the French SPOT satellite. There, the detecting row will contain more than 500 elements.

The operating principle of these sensors is the following:

The sun's image is formed by a lens on a light-detecting strip (figure 16). Regular sampling of the accumulated charge makes it possible to locate the sun's edges by a system of thresholds (transition from 0 to 1 and from 1 to 0).

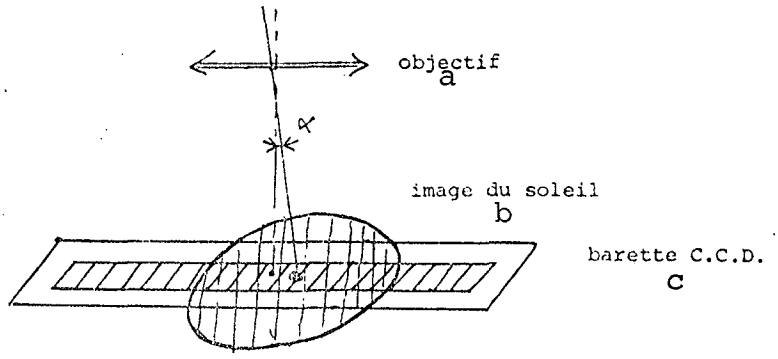

Figure 16

Key: a) objective
b) the sun's image
c) CCD row

In practice, the information can be read rapidly (every millisecond, for example). One can thus combine the successive measurements and eliminate the quantization effect if the sun's image changes in relation to the strip.

Typical precision: 0.005 degree for a ± 10° field.

5.2 Examples of Star Sensors

A large number of star sensors have been developed in the United States. Some of them track the stars mechanically, but in this course we are mainly interested in electronic scanning star sensors. These include the image dissector star sensor and star sensors using CCD rows and mosaics. /339

A description of the image dissector has already been given and the Sodern image dissector sensor is described in the course on "the space shuttle's pointing system". We will therefore speak here about CCD star sensors.

Example 1: the CCD Row Star Sensor Developed at RAE (UK)

A lens with a focal length close to 30 cm forms the stars' images on a CCD row of 1,024 elements. The row's integration period is 25 ms. It allows the detection of stars having a visual magnitude of 4 with a signal-to-noise ratio of 18.

Two pieces of information are useful with this type of sensor:

1) The angle between the optical axis and the direction of the detected star, as given by the number of the detecting element.

2) The instant the star passes through the plane containing the optical axis and the middle of the strip.

For a 3° field of view, the precision on each axis is about 10 arc seconds (3σ), for a maximum bias of 10 arc seconds (field of view: 3°).

Example 2: CCD Mosaic Star Sensor Developed at JPL (USA)

This type of sensor, named STELLAR, is in fact the equivalent of an image dissector star sensor. It uses a 100 x 100 CCD mosaic (in the experimental model). The precision is 10 angular seconds in a 3° x 3° field. To guarantee the precision, it can simultaneously follow ten stars with a visual magnitude of less than or equal to 6. An Intel 8080 microprocessor collects and processes the data from the actual star sensor itself.

5.3 Examples of Earth Sensors

5.3.1 IR Thermopile Earth Sensor

We shall briefly describe the static SYMPHONIE sensor with the purpose of pointing out the sources of error. We shall then see how the performance has been improved with the OTS static sensor.

Figure 17 shows a schematic drawing of the sensor.

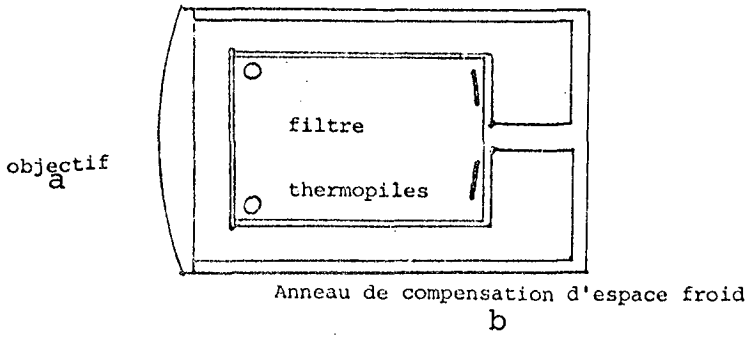

Figure 17

Key: a) objective
b) Cold Space Compensation Ring

An outer air-tight housing holds the germanium objective. The /340
inner housing holds the filter, the cold space compensation ring, and the thermopiles.

The image of the earth is formed on the thermopiles, which are arranged as indicated in figure 18.

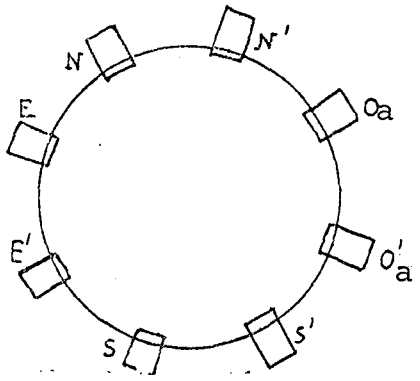

Figure 18

Key: a) W[est]

The N-S thermocouple pair mounted in opposition to each other constitutes a channel. The N'S', EO, and E'O' pairs make up other channels.

There are four channels available for information on east-west and north-south displacement. There are therefore always two channels free which are used for:

-- providing redundant channels for times when the sun disturbs the functioning of a channel;

-- controlling cold space compensation. In this case, the two thermopiles' signals are added, rather than subtracted.

Role of Cold Space Compensation

In the nominal position, the portion of the thermopile surface covered by the earth is small. This is done to avoid too large pointing errors caused by variations in the earth's luminance.

Each thermopile therefore mostly exchanges with the depths of space. Because of this, the thermopiles tend to produce a very large negative signal that is proportional to their sensitivity.

The sensitivity (S) of two paired thermopiles is never exactly identical. Thus, in the absence of any pointing error, the more the thermopiles are cooled, the greater the channel's signal is. This error can be reduced by heating the two thermopiles equally.

The difficulty comes from the fact that the thermopiles' sensitivity is not a uniform function of wavelength. They emit in the 14-16 micron channel (filter) and are heated by the whole spectrum. Assuming that each thermopile receives the same quantity of energy from the ring, it must be that

$$\left(\frac{S_1}{S_2}\right)_{14\text{-}16\ \mu m} = \left(\frac{S_1}{S_2}\right)_{\text{the whole spectrum}}.$$

The selection of thermopiles is made even more difficult by the /341
fact that all the channels must have identical characteristics if they are to be connected without distorting the data.

The distortions are due to:
-- the variation in the earth's luminance;
-- the temperature gradient in the thermopile support structure.

In addition, commutation of channels must not result in discontinuities. Commutation may be done to:
-- replace the channel over which the sun is going to pass: there is a sun sensor which signals the sun's arrival;

-- use the wettest channel, i.e. to minimize the effect of transverse pointing errors.

Precision: better than 0.3°

The OTS Sensor

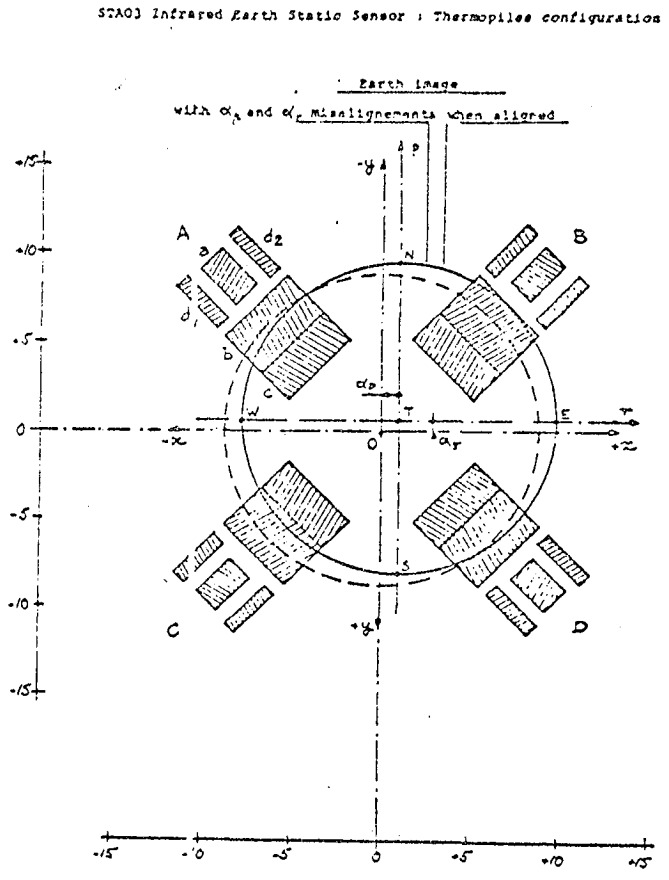

Figure 19

The arrangement of thermopiles in the OTS sensor is given in figure 19.

Each thermopile is made up of 5 elements, a, b, c, d_1, and d_2. For acquisition, a + b + c is formed. Cold space compensation is controlled by $d_1 + d_2$. For fine pointing, b - (a + c) is recorded.

The big difference from Symphonie is that a large part of the effect of luminance variation on each thermopile is eliminated.

Mode of operation with four thermopiles:

Roll $v_p = A + B - (C + D)$
Pitch $v_p = A + C - (B + D)$

Mode of operation with three thermopiles:

Example: A suppressed, $V_p = B - D$; $V_p = C - D$.

Finally, the thermopile support block has a thermostat to eliminate any risk of a temperature gradient appearing.

Precision: better than 0.05° for a pointing error of less than 0.25°.

5.3.2 IR Horizon Scanning Sensor /343

This type of sensor generally uses a bolometer as the detector. In spinning satellites, the movement imparted by the satellite is sufficient to assure the horizon detector's operation. In three-axis stabilized spacecraft, it is necessary to move the earth's image on the detector with the aid of an oscillating mirror (Galileo sensor), rotating prism (TD earth sensor), or a rotating mirror (ANS earth sensor).

A schematic diagram of the plane scanning earth sensor on-board the Dutch ANS astronomical satellite is displayed in figure 20. This sort of sensor makes it possible to detect the earth's horizon with a precision of a few tenths of a degree in low orbit (500 to 1500 km).

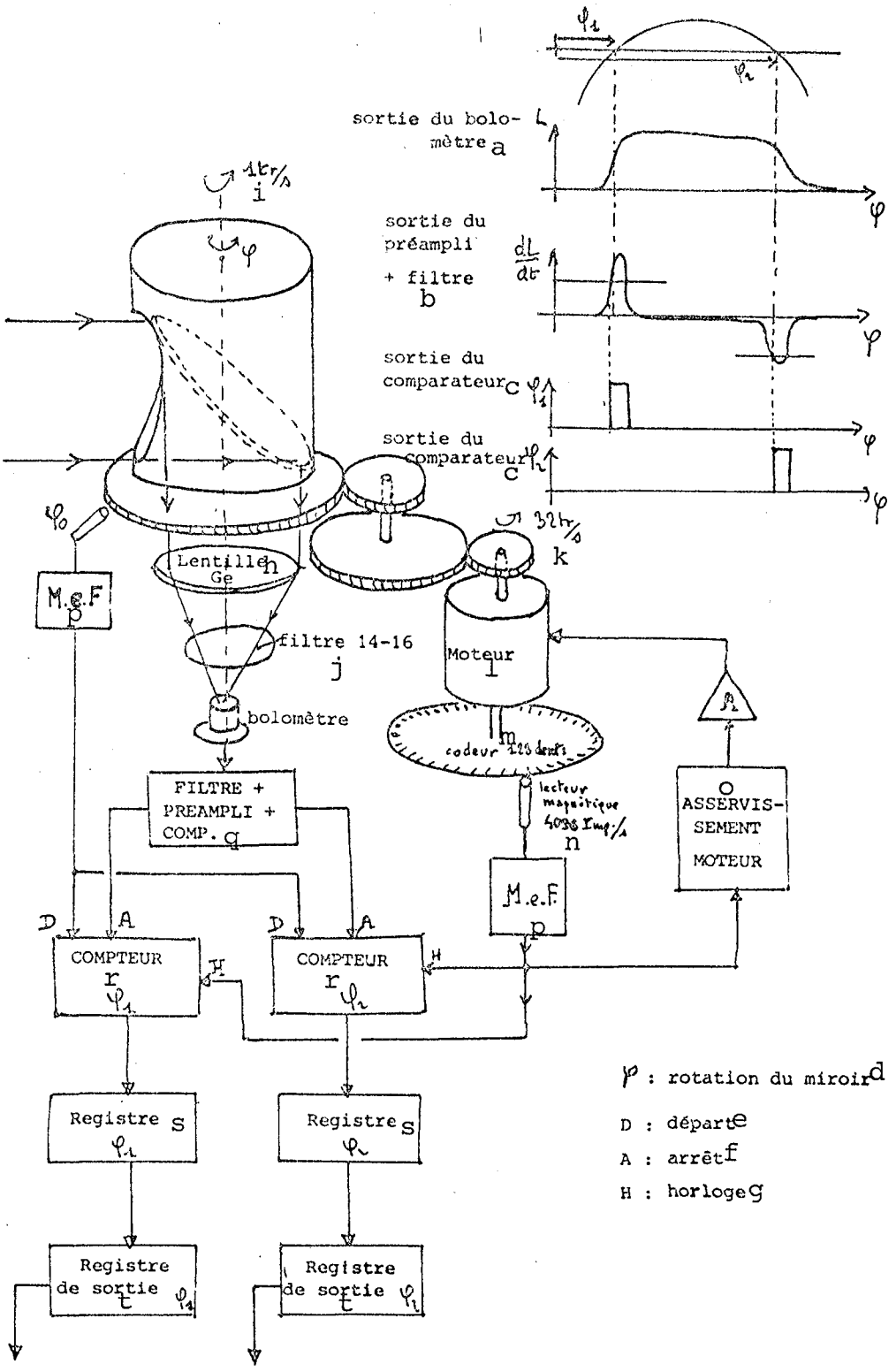

Figure 20
Schematic Drawing of ANS Horizon Sensor

(The key will be found on the following page.)

Key to figure 20:

a) bolometer output
b) preamp + filter output
c) comparator output
d) ϕ = rotation of mirror
e) D = start
f) A = stop
g) H = clock
h) Ge lens
i) 1 rev/sec
j) 14-16 micron filter
k) 32 rev/sec
l) motor
m) 128 tooth encoder
n) magnetic reader, 4096 pulses/sec
o) motor servocontrol
p) M & F
q) Filter + Preamp + Counter
r) Counter
s) Register
t) Output Register

The signal issuing from the detector in such a sensor is the result of the combination of three functions:

-- the earth's luminance along the scanned chord,

-- the field of the detector,

-- the detector's pulse response.

The error in measuring ϕ_1 and ϕ_2 is made up of:

-- quantization uncertainty: 360/(2 x 4096) = 0.44° max;

-- uncertainty due to the variations in the earth's luminance: 0.07° max;

-- noise: 0.21° at 3σ;

-- pseudo-constant bias: 0.05° max.

5.4 Magnetic Sensors

We mention the three-axis magnetometers only so that they may be kept in mind. Some of them are capable of plotting the magnetic field with a precision of 1/1000 of its amplitude (precision of 1/10 degree). Their limitations arise mainly from uncertainty in our knowledge of the magnetic field and its fluctuations.

5.5 Example of an Inertial Gyroscope Sensor

Let us return to the gyroscope equation of section 4.3.1:

$$H\omega_i - I(d\omega_o/dt) - f\omega_o - \Gamma_m = 0$$

At low frequencies ($f < 10$ Hz), the effect of inertia, $I(d\omega/dt)$ can generally be neglected. This results in the following open loop gyroscope block diagram:

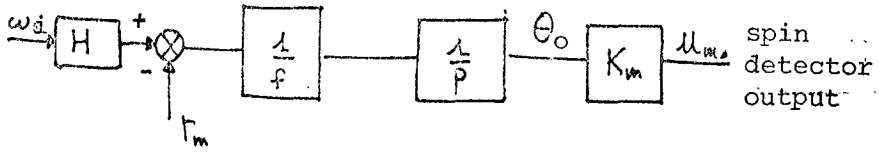

(motive torque)

In closed loop systems, integral feedback keeps the detector centered on the null point. A phase advance network is also added: /345

$$\frac{1 + T_1 p}{(1 + T_2 p)(1 + T_3 p)}$$

which results in the following closed loop block diagram:

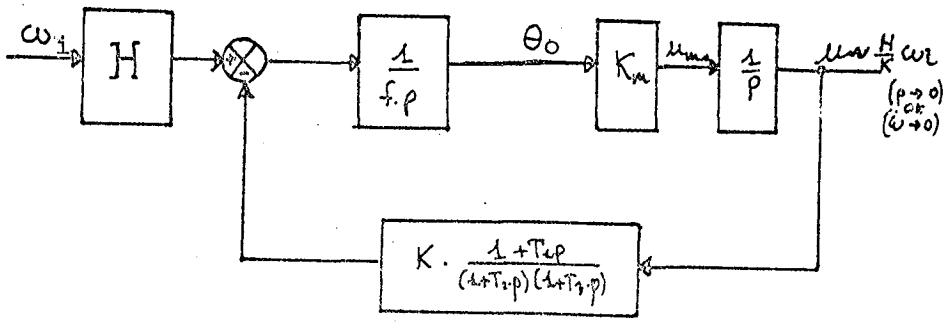

and the following transfer function:

$$\frac{u}{\omega_i} = \frac{H \cdot Km}{f} \cdot \frac{(1 + T_2 p)(1 + T_3 p)}{p^2 (1 + T_2 p)(1 + T_3 p) + \frac{Km}{f} \cdot K \cdot (1 + T_1 p)}$$

The T_1, T_2, T_3, and K coefficients are adjusted to obtain stability with the desired passband. (It is important to eliminate certain frequencies induced by the rotor's rotation. If needed, a filter is added to the gyroscope output to further attenuate these frequencies.)

Example: In the case of a SAGEM type F gyroscope incorporated into an attitude sensor and for a 1 Hz passband, the random drift is on the order of 0.3°/h at 3σ.

6. Sensor Combinations for Obtaining Total Attitude

We shall limit ourselves here to systems for measuring attitude in three-axis stabilized vehicles pointed geocentrically and, more precisely, locked into the local orbital reference system.

We have chosen two examples:

1) The attitude measurement system proposed for the SPOT earth observation satellite, which uses 1 (or 2) earth sensors, 1 fine sun sensor, and 3 gyros (no redundancy).

2) The attitude measuring system developed at RAE (UK) that uses both gyros and a CCD star sensor. /346

6.1 SPOT Attitude Measurement System (without Redundancy)

This satellite is placed in a heliosynchronous circular orbit with an 800 km altitude and a local time of 10:30 PM (first mission). It uses two ANS-type scanning earth sensors (conical scanning), which

makes it possible to plot the satellite's angles of pitch and roll with the aid of angular information on the space-earth and earth-space transitions (ϕ_1, ϕ'_1) and (ϕ_2, ϕ'_2), provided by the sensors (see figure 21).

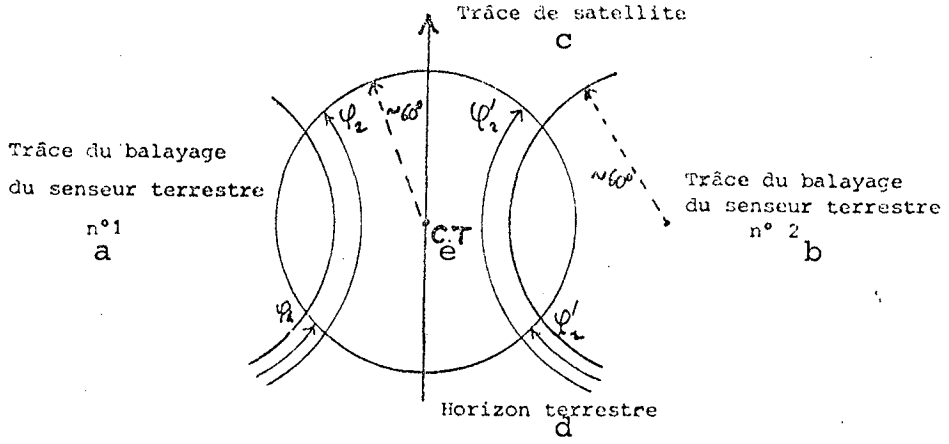

Figure 21

Key: a) Earth Sensor Scanning Trace No. 1
b) Earth Sensor Scanning Trace No. 2
c) Satellite Trace
d) Earth's Horizon
e) C.E.

Two fine single-axis digital sun sensors (see section 5.1) give the angle of yaw every half-orbit by finding the angle between the sun and its projection on the orbital plane.

Finally, three gyros connected to the structure measure the satellite's angular velocity around the three axes. Integration of the gyroscopic measurements and the resetting of the gyros by the optical sensors results in satellite attitude measurements to about the nearest 0.1° along the three axes.

(See figure 22 for a schematic diagram of the SPOT attitude measurement system.)

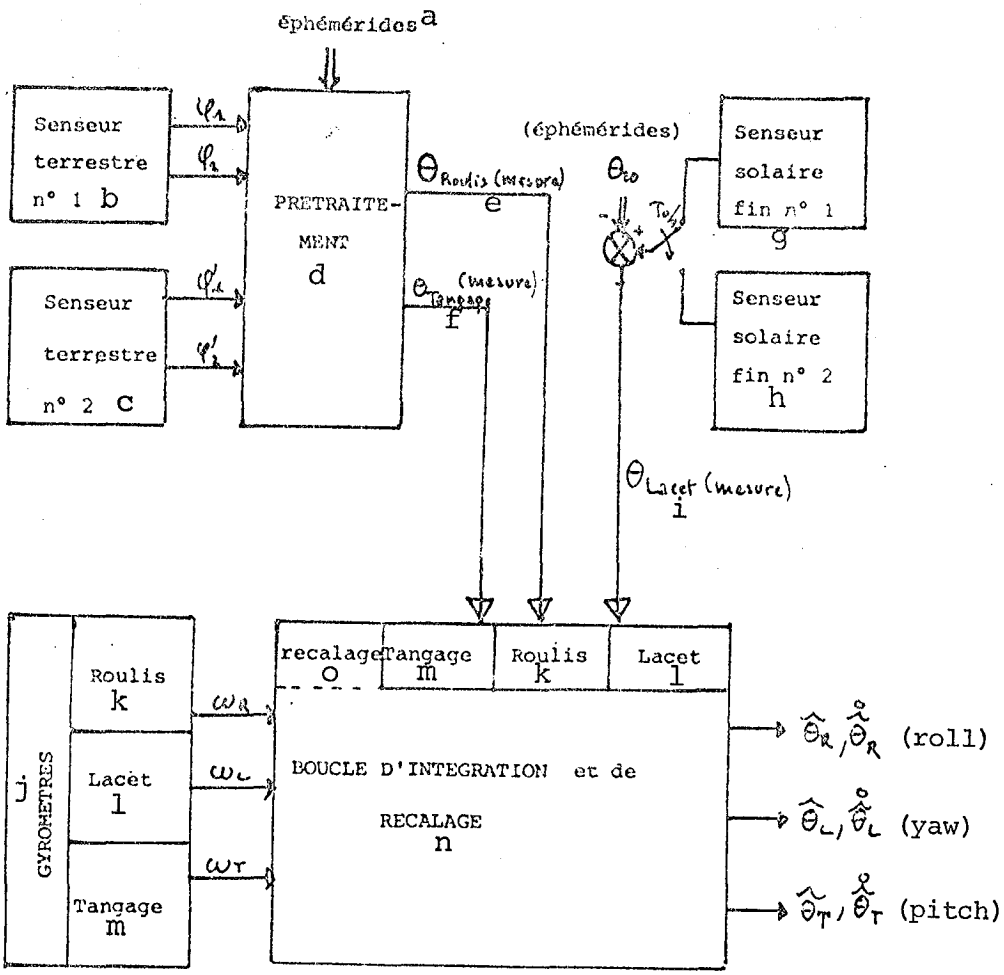

Figure 22
Schematic Diagram of the SPOT Attitude Measurement System

Key:
a) ephemerides
b) Earth Sensor No. 1
c) Earth Sensor No. 2
d) Preprocessing
e) θ (roll) measurement
f) θ (pitch) measurement
g) Fine Solar Sensor No. 1
h) Fine Solar Sensor No. 2
i) θ (yaw) measurement
j) Gyros
k) Roll
l) Yaw
m) Pitch
n) Integration and Reset Loop
o) reset

6.2 Combined CCD Star Sensor and Gyro Attitude Measurement System

This system uses a 1024-point CCD strip star sensor, briefly described in section 5.2, and three strapdown gyros (no redundancy). The star sensor's optical axis is at 45° from the pitch axis (nearly perpendicular to the orbit).

For a satellite locked onto the local orbital reference system, and therefore slowly rotating about the normal to the orbit at the orbital angular velocity $\omega_o = 2\pi/T_o$ ($\simeq$ .001 rad/sec), the star sensor's field of view scans the space located between two cones and thus regularly intercepts stars (see figure 23).

An average of fourteen transitions involving stars with a magnitude of less than four are thus observed per orbit (for low orbits). /348
In addition to each star's intensity, the sensor also supplies the time of passage and the angle between the direction of the star and the axis of pitch. This information provides the basis for resetting the gyros (see figure 24). The attitude about the three axes can thus be measured to the nearest one-hundredth degree.

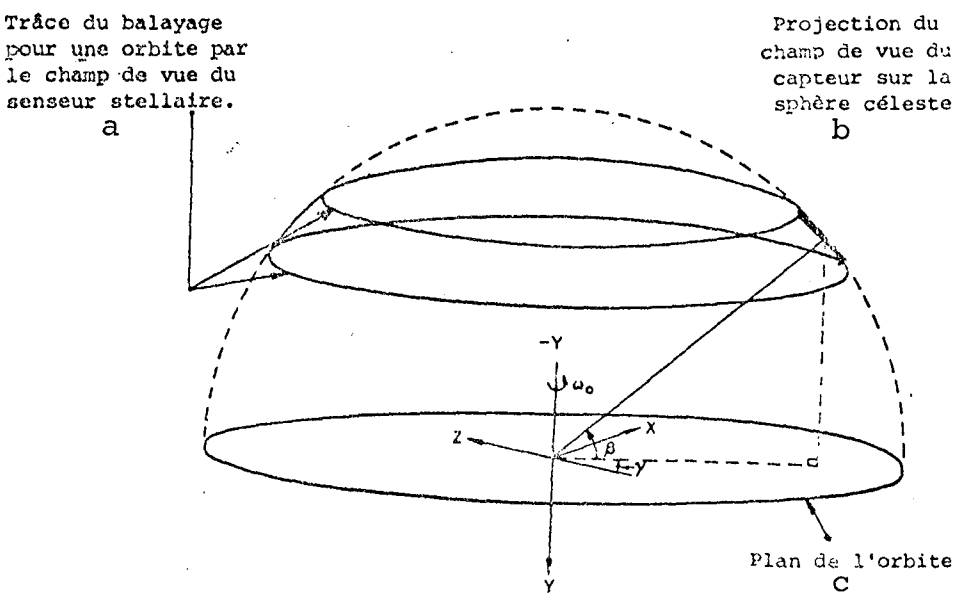

Figure 23

(Key to this figure will be found on the following page.)

Key to figure 23:

a) Area scanned during one orbit by the star sensor's field of view.
b) Projection of sensor's field of view on the celestial sphere.
c) Orbital Plane.

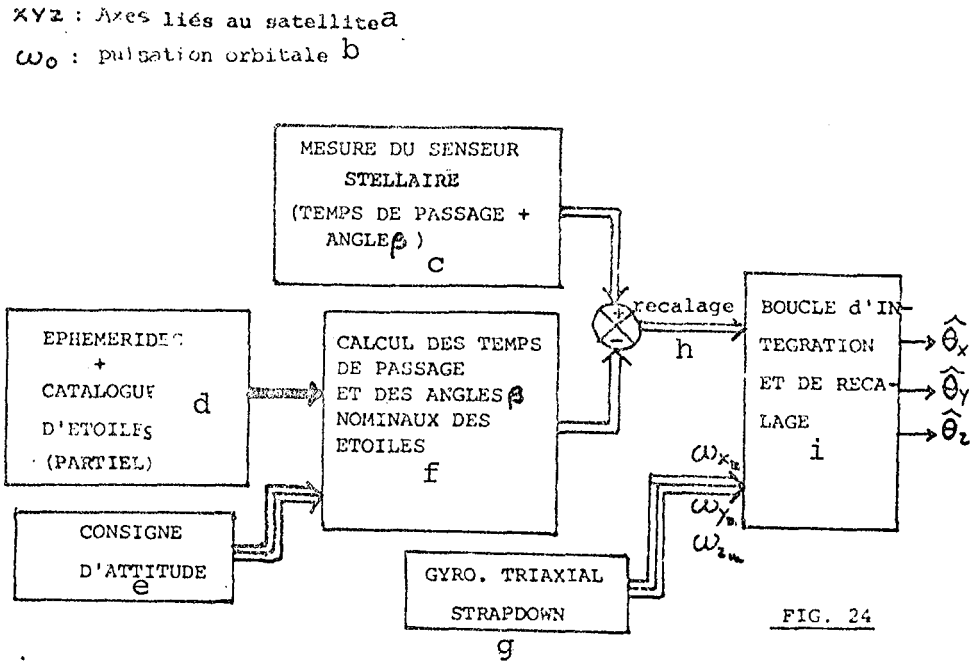

Figure 24

Key:
a) xyz: satellite axes
b) ω_o: orbital pulsatance
c) Star Sensor's Measurements (Time of Passage & Angle β)
d) Ephemerides & (Partial) Star Catalogue
e) Attitude Instructions
f) Calculation of Nominal Angles of and Times of Passage for Stars
g) Three-axis Strapdown Gyro
h) Resetting
i) Integration and Resetting Loop